

# Electron-detachment cross sections for $O^- + N_2$ near the free-collision-model velocity threshold.

A. A. Martínez,<sup>1</sup> M. M. Sant'Anna,<sup>2</sup> and G. Hinojosa<sup>1,\*</sup>

<sup>1</sup>*Instituto de Ciencias Físicas. Universidad Nacional Autónoma de México, Apartado Postal 48-3, Cuernavaca 62251, Mexico.*

<sup>2</sup>*Instituto de Física, Universidade Federal do Rio de Janeiro, Caixa Postal 68528, Rio de Janeiro, 21941-972, RJ, Brazil*

We present measurements of the total projectile-electron-loss cross sections in  $O^- + N_2$  collisions in the energy range from 2.5 to 8.5 keV. Two different techniques, beam attenuation and the growth rate, are employed. The difference between the values obtained with the two methods is explained under the hypothesis of a contribution from anionic metastable auto-detaching states. Under this hypothesis, the long-standing question of a strong disagreement among reported measurements at the low-energy range is also explained. The cross sections measured using the growth-rate method show a threshold behavior. We analyze the cross-section velocity dependence in the framework of a collision between a quasi-free electron, loosely bound to the projectile, and the molecular target. Within the free collision model, we deduce and test a simple analytical expression for the expected velocity threshold taking into account the angular distribution of electron velocities within the anion.

## I. INTRODUCTION

In negative ions, the extra electron is bound to its neutral core by weak Coulomb-screened potentials and by electron correlation effects. For this reason, both structure and collision models, even for the simplest cases, demand highly electronically correlated approaches and are, in turn, a severe test-bed for state-of-the-art theoretical methods. Such may be the case of the realization of negative methane [1] and the extremely long-lived  $CCH_2^-$  anion [2].

Negative ions are, in general, an important species in Nature. Its presence in cold plasmas [3, 4] is relevant to the electronic density function since they are a source of thermal electrons. In atmospheric environments, anions were found in the upper atmosphere of Titan satellite [5], in the coma of comets [6], and are of importance in artificial atmosphere generation [7]. In the case of the interstellar medium (IM) [8], despite the hostile conditions for their permanence, negative ions are abundant and a well-established fact. Understanding their presence in the IM constitutes a current question in science [9]. Even in the well-established field of small-mass spectrometry, a newly negative ion species (of  $m/q = -16$ ) has been reported [1, 10]. These questions prompt the need for more fundamental studies about this kind of ions and their interactions. Particularities of negative-ion projectiles, when compared to the more simple positive-ion or atomic projectiles, are observed in the search for scaling laws for projectile-electron-loss cross sections [11–16].

Even for a projectile as simple as an electron, scattering by the  $N_2$  target show a large variety of involved processes [17]. When the projectile has internal structure, and the high degree of electronic correlation characteristic of anions, the complexity of the collision sys-

tem increases significantly. In this work, we present measurements of electron-detachment cross sections for the  $O^- + N_2$  collision system. The measurements support an explanation, based on the possible unnoticed production of autoionizing states during experiments, for a long-standing discrepancy among reported cross section data at energies of few keV.

The velocity range of the cross sections reported here allows a study of the onset of a projectile-electron-loss mechanism with a quasi-free-electron behavior. The experimental data measured with the growth rate method present a velocity threshold. We show that the threshold value is consistent with the estimate of the free collision model (FCM), taking into account energy and momentum conservation and the angular dispersion of a quasi-free electron within the anion. A general and simple analytical expression for this FCM threshold velocity is presented and tested with the  $O^- + N_2$  collision system.

## II. EXPERIMENT

The experimental method used here has been described in previous publications [18–20]. The method consists of the application of two different well-established techniques, namely, beam attenuation (BAT) and signal growth rate (SGR). Both techniques are used rather than one alone. This offers an improved insight, given that the physics from each technique can be different, as explained ahead. In short, the method is based on measuring the remaining negative ions from an  $O^-$  ion beam after their interaction with  $N_2$  gas (BAT), or the resulting neutral atoms of oxygen resulting from the electron loss from the  $O^-$  ion-beam interaction with  $N_2$  (SGR). Following, we present a self-standing description of the experimental method with emphasis on the present study.

In the initial stage, an ion beam of negative oxygen ions is produced. This was carried out by introducing

---

\* Corresponding author: hinojosa@icf.unam.mx

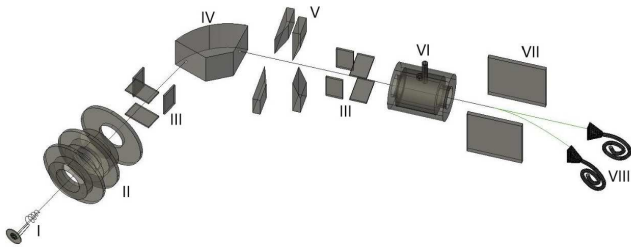
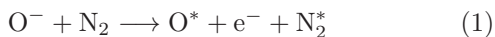


FIG. 1. Schematic diagram of the apparatus. Not presented to scale. I, This filament is inside a small quartz chamber (not shown). II, electrostatic lens set. III, steering plates. IV, magnet sector. V, collimating slits. VI, gas-cell. VII, analyzing parallel plates (PP). VIII, Particle counters or channel electron multipliers (CEMs).

a combination of argon and carbon dioxide gases into a cylindrical chamber made of quartz containing a tungsten filament that was heated to incandescence. The pressure in this chamber was monitored not to exceed the order of  $10^{-1}$  Torr. At one end of the quartz chamber, a metallic cap with a centered 1.5 mm diameter orifice had a 100 V voltage applied to it in order to accelerate negatively charged particles. Electrons ejected by the filament suffered this acceleration and, in turn, interacted with the gas mixture producing a plasma [10] from which negative ions could be extracted. The assembly containing the chamber was biased to the acceleration voltage. Negative ions from the plasma were expelled through its orifice and in turn repelled or accelerated toward a focusing electrostatic lens set, yielding to a magnetic field where the ions are separated according to their momentum and electric charge, thereby resulting in a mono-energetic, mass-analyzed ion beam. After the magnetic-field region, the ion beam passes through a set of collimating slits to control its width and therefore its intensity. These slits were mounted on linear motion feed-throughs in such a way that the ion beam could be scanned in both directions at right angles on the normal plane to the ion-beam trajectory, and hence be able to monitor its profile too. Before and after the magnetic field's region, two sets of parallel plates (PP), installed perpendicularly to the ion-beam direction, were used to apply small electric fields to further, fine-tune the ion-beam trajectory towards a gas cell. The gas cell was built with input and output collimator orifices with diameters of 1.0 mm and 1.5 mm respectively, and with a length of 6 cm.

Overall, a single species, mono-energetic, collimated, and focused beam, with a width of  $\approx 0.5$  mm, enters a gas cell where the interaction of  $O^-$  and  $N_2$  occurs in a time-frame of a fraction of  $10^{-15}$  s,



where the star is used to indicate an unknown final internal state. High-purity  $N_2$  gas was used. The resulting

neutral oxygen atoms continued in their original trajectory towards a channel electron multiplier (CEM) located in the symmetry axis of the apparatus. The remaining  $O^-$  ions from the parent ion beam were separated by a perpendicular electric field set to steer the ions toward a second CEM installed off-axis of the accelerator symmetry axis. This electric field was generated with a set of parallel plates (shown in Fig. 1 labeled as PP).

The time of flight of an  $O^-$  ion from the output of the ion source to the entrance of the gas cell was of the order of  $\mu s$ . The experiment was performed under high vacuum conditions so that the mean free path of the ion beam was, at all times, larger than its total trajectory.

To verify if there was a full collection of charged particles, the ion-beam intensity was measured as a function of the PP's electric field. This produced a profile of the ion beam as a function of the PP voltage that systematically showed a distribution with a plateau, thereby showing that the ions were fully collected because their spread was smaller than the width of the CEMs acceptance aperture after dispersion in the gas-cell. The CEMs collecting apertures were rectangular with dimensions of 7 mm (width) and 15 mm (height).

As a test for the neutral atoms collection, we executed a check performed in another experiment done with the same apparatus and with a lighter  $H^-$  ion-beam [20] under similar experimental conditions. In that experiment, the distance between the gas cell and the detectors was changed between two experimental campaigns providing a difference in the aspect ratios (detector's width to distance from the gas cell) of about 18%. This resulted in no measurable difference between the two sets of electron-loss cross sections, thereby, verifying that the different amounts of collected neutral atoms were not measurable.

To verify that both CEMs had the same detection efficiencies, the counting rate in the central CEM was measured with the PP electric field set to zero, corresponding to a total count rate of residual neutral atoms plus the  $O^-$  parent ion-beam counts. With the PP electric field on, the lateral CEM count rate (parent ion beam) plus the central CEM count rate (residual neutral atoms) was checked to add up to the total count rate in the central CEM. This check was performed under empty gas-cell condition. The CEMs' bias voltage gains were also slightly adjusted for maximum counting rates and the count rates were kept below  $1 \times 10^4$  s $^{-1}$  as to guarantee optimal performance of the CEMs.

Systematic errors originate from uncertainties in gas-cell pressure and temperature measurements that propagate a maximum of 11% uncertainty to the cross-section measurements. The relative pressure in the gas cell was monitored with a Baratron capacitance manometer. The kinetic energy had a maximum of 5% uncertainty. In the ion source chamber the base pressure was  $8 \times 10^{-4}$  Pa without gas load, and  $5 \times 10^{-2}$  Pa with gas load. The detection chamber pressure was  $5 \times 10^{-5}$  Pa.

Total electron-loss cross sections were derived from the total count signal measured in each of the CEMs (cen-

tered and lateral) as a function of the  $N_2$  gas target thickness ( $\eta$ ). Using the signal from the neutral atoms of oxygen (centered CEM) we applied the signal growth rate method (SGR), and with the signal in the lateral CEM, we applied the beam attenuation technique (BAT).

The target thickness  $\eta$  of the  $N_2$  gas in the gas-cell is defined as

$$\eta = \frac{\ell P}{\kappa T}, \quad (2)$$

where  $\ell$  is its effective length,  $P$  the pressure and  $T$  the temperature of the gas cell.  $\kappa$  is Boltzman's constant.

The SGR method is based on the solutions to the equilibrium equations for the fraction of neutral particles to the number of anions in the ion beam  $F_0$  as a function of the target thickness  $\eta$ .  $F_0$  was derived from

$$F_0 = \frac{I_0 - I_b}{I_i}, \quad (3)$$

where  $I_0$  is the signal count rate of oxygen atoms that resulted from the interaction with the gas,  $I_b$  is the ion-beam background count rate resulting from the ion-beam interaction with the residual vacuum system and  $I_i$  is the count rate corresponding to the parent ion beam. The SGR method is described in more detail in the references [21–23]. In this method, the fraction  $F_0$  of neutral particles formed after the ion-beam loses an electron by collisions with the gas is a function of the initial parent ion-beam intensity and the target thickness. The single-detachment cross section  ${}^s\sigma_{-10}$  was derived from the first-order approximation to  $F_0$

$$F_0 = {}^s\sigma_{-10}\eta, \quad (4)$$

where  ${}^s\sigma_{-10}$  is the single collision detachment cross section measured with the SGR method and  $\eta$  is the target thickness.

Examples of a growth rate curve and a beam attenuation curve of the present work are shown in Fig. 2. All measurements were carried under single collision conditions, *i.e.*, when the functional dependence of the normalized signals to  $\eta$  was linear. Under these conditions, higher-order effects are expected to be negligible.

The beam attenuation technique (BAT) consists of measuring the decline of the parent ion-beam intensity as a function of the gas thickness  $\eta$ . The cross section was derived from:

$$I = I_0 \exp(-{}^b\sigma_{-10}\eta), \quad (5)$$

where  $\eta$  is given by Eq. (2),  $I$  is the ion beam intensity as a function of  $\eta$  and,  $I_0$  is the initial intensity of the ion beam.  ${}^b\sigma_{-10}$  is the total electron-detachment cross section. An example of a BAT curve for the present data

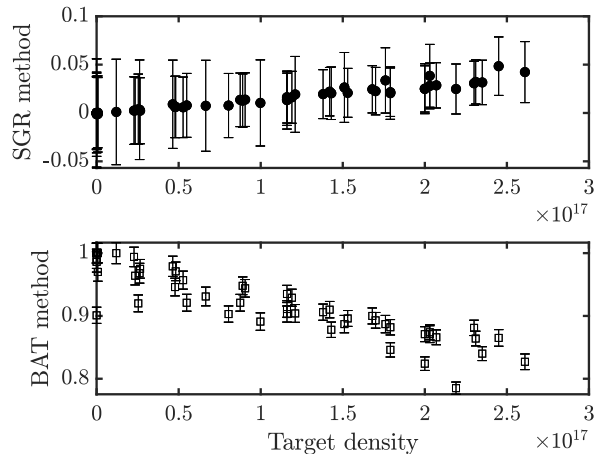


FIG. 2. Examples of the measured data at 5 keV. Top panel corresponds to the reduced data for the SGR method:  $F_0$  as a function of the target thickness  $\eta$  in Eq. 4. The bottom panel corresponds to BAT:  $I/I_0$  as a function of  $\eta$  in Eq. 5.

is shown in Fig. 2. The BAT technique has been used and described in more detail in the references [24, 25].

The dispersion of the data in Fig. 2 is mainly caused by the instability in the ion-beam intensity, originated by plasma fluctuations in the ion source. In the case of BAT, the vertical axes of Fig. 2 correspond to the ion-beam intensity readings normalized to  $I_0$ . In the case of SGR, the vertical axis correspond to the average of the initial and final ion-beam currents. This could be the reason for the difference in the data dispersion. Data sets where the ion-beam intensity differed by 10% or more during the beginning and the ending of an experimental measurement were discarded.

Once a distribution of cross-section values was obtained at each energy, standard deviations were derived as a measure of the statistical errors, that were in turn combined with the systematic uncertainty to derive total errors per energy point. Our whole set of data was normalized by a single constant factor so that our cross-section data point measured at 5 keV using SGM coincides with the 5 keV correspondent value also measured using SGM by Matic and Covic [26].

### III. RESULTS AND DISCUSSION

The present data are shown in Fig. 3. Data points correspond to the beam attenuation technique or BAT (open data points), and to the signal growth ratio or SGR (closed data points). In the figure are also plotted data from Bennet *et al.* [27], measured with BAT, and data from Matic and Cobic [26], measured with SGR.

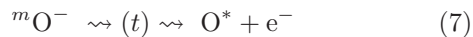
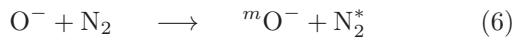
At first approximation, BAT and SGR cross-sections are expected to have similar values, given that the ion beam composition is only of  $O^-$  ions and that the de-

pendence of the signals with target density is under single collision conditions. However, the cross sections measured with each technique are very different. This kind of disagreement at the low energy interval has been a question in the field and is not restricted to the  $O^- + N_2$  collision system [28].

It is important to note that by using BAT the total decrease of the  $O^-$  ions from the ion beam is measured, therefore all processes that may cause a reduction of the ion-beam intensity are accounted for. By using SGR method, only neutral atoms resulting from the interaction with  $N_2$  are detected, which means that processes that produce neutral atoms in the direction of the ion beam are accounted for.

This difference may be caused by a process that is not measured in the SGR method and influences mainly the BAT cross-section for  ${}^b\sigma_{-10}$  to be larger than  ${}^s\sigma_{-10}$ . One aspect of the data is that the difference in the cross sections seems to decrease as the interaction energy increases. We note that as the kinetic energy increases, the time of flight within the apparatus becomes shorter. A possible explanation consists of the presence of auto-detaching states (AD) of  $O^-$  that release the electron in its path to the lateral CEM and in the electric field of the PPs. As the time of flight becomes longer in the low energy interval of the present study, the AD states are more likely to deplete the  $O^-$  population in its trajectory to the detector, and as a consequence,  ${}^b\sigma_{-10}$  becomes larger than  ${}^s\sigma_{-10}$ .

This tendency may be consistent with the presence of a time-dependent process,



where the star is used to indicate an undetermined final state and the super index  $m$  in  ${}^mO^-$  is used to designate a metastable auto-detaching state. Therefore, to explain the difference between the cross-sections, we propose the next hypothesis: Metastable states that auto-detach after the collision contribute more to  ${}^b\sigma_{-10}$  cross section because the extra electron can also be lost in its trajectory to the lateral CEM.

Other processes involved in the interaction may be direct electronic detachment, electron transfer (ET), double detachment (DD) and single detachment followed by electron transfer where the final state is  $O^0$ . However, the last process would imply secondary collisions and can be ruled out from single collision conditions (see Fig. 2).

In the case of DD channel, its contribution has been measured to be negligible for other collision systems [29, 30], and for  $O^- + N_2$ , in particular, [26]. In this experiment, we measured the relative contribution of the resulting  $O^+$  yield by reversing the polarity of the PP showing a very low counting rate of, at most, one order of magnitude lower when compared to the intensity of the SGR signal. This demonstrates that the DD channel contribution cannot justify the difference. In the case of

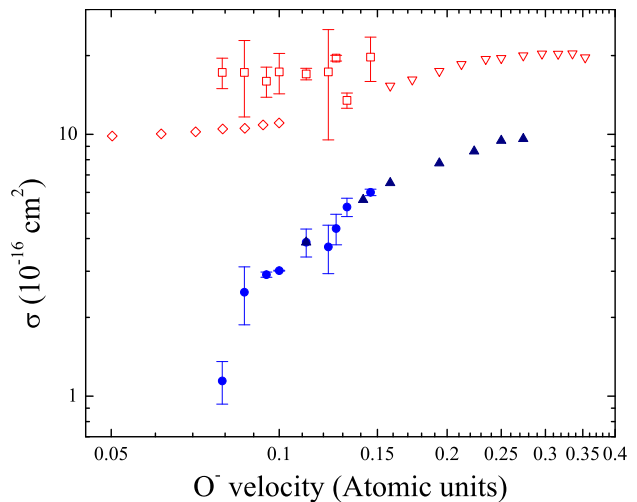


FIG. 3. Total electron-loss cross sections for Eq. 1. Data measured with BAT, open squares: present work; diamonds: Bennet *et al.* [27]; inverted triangles: Tsuji *et al.* [32]. Data measured with SGR, closed circles: present work; up triangles: Matic and Covic [26]. Error bars for the present data correspond to total errors, standard deviation, and systematic uncertainties. Errors for cited work are not plotted.

ET, this process cannot be separated by these methods and its contribution is expected to have the same effect in both techniques.

Another possibility is electric field-induced detachment. This possibility is discarded on the next bases: a procedure in this experiment consisted in verifying the detectors to have similar efficiencies. This was carried out by measuring the count rates with the electric field on and off, and without gas load in the gas-cell. This shows that the electric field alone did not induce measurable electron detachment. Consistently, the PP electric field intensity resulted inchoate ( $< 300 \text{ V cm}^{-1}$ ) to induce electron detachment [31].

Figure 3 shows that the present BAT data are consistent with data from Bennet *et al.* [27] and Tsuji *et al.* [32], measured with the same method. For the case of the cross sections measured with the SGR method, the present data agree with the results from Matic and Covic [26] in the coincident energy range from 5 keV to 8.5 keV. The apparent disagreement between both sets of data previously published for the process of Eq. (1) has been solved under the hypothesis stated above.

We hasten to note that BAT cross-sections are consistent in the sense that their values fall within close order of magnitude scales. However, they disagree. Yet, this is congruent with the hypothesis of auto-detaching metastable states, because the cross-section values would depend on the time of flight within the machine.

We introduce the idea that AD states  ${}^mO^-$  form as



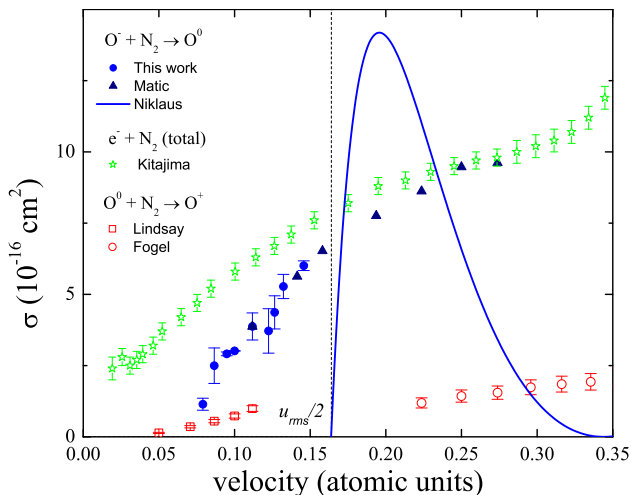


FIG. 4. Cross sections for processes relevant to the free-electron-model hypothesis for the present interaction system. Open stars: electron-scattering cross sections  $e^- + N_2$  of Kitajima [33]. Electron-detachment cross sections for neutral projectiles  $O^0 + N_2$ : open squares, Lindsay [34]; open circles, Fogel [35]. Electron-detachment cross sections for anionic projectiles  $O^- + N_2$ : closed up triangles, Matic [26]; closed circles, present SGR data; line, Eq.(8). Vertical dotted line:  $O^-$  velocity given by Eq. (12).

a result of the collision with the  $N_2$  gas target. Then, these states may decay along their trajectory from the gas cell to the CEM detectors. When they pass through the electric field between the PP analyzing plates, they continue to decay at their natural rate and may not be detected by the central CEM.

In Fig. 4 we compare data for  $O^- + N_2$  single-electron-detachment cross sections measured by SGR method and with cross sections for two related projectiles incident on  $N_2$ : electrons and atomic oxygen. The total electron scattering cross sections for  $e^- + N_2$  agree with the data for  $O^- + N_2$  at  $v \sim 0.25$  a.u., showing that above this velocity the description of the anion as a quasi-free electron plus a neutral core is meaningful for the  $O^- + N_2$  detachment collision channel. The comparison between  $O^- + N_2$  and  $O^0 + N_2$  electron-detachment cross sections also supports the quasi-free electron picture. The  $O^0 + N_2$  cross sections are much smaller than the  $O^- + N_2$  equivalent velocity ones, suggesting a dominating contribution of the loosely-bound electron in an  $O^- + N_2$  electron-plus-core simplified modeling of the anionic projectile.

In order to estimate projectile-electron-loss cross sections, Bohr and Lindhard [36, 37] calculate the cross section for energy transfer greater than  $T$  in a collision between a free electron at rest (in the projectile's frame of reference) and a heavy particle (the target) with charge  $Z_{ef}$ , where  $T_{max} = 2mv^2$  is the upper limit for energy

transfer in such a collision. Thus, in this approach, the neutral target is modeled as a dressed charge that ionizes the electron loosely bound to the projectile. Niklaus *et al.* [38, 39] include in the Bohr-Lindhard version of the FCM an empirical velocity-dependent effective charge  $Z_{ef}(v)$  and obtain

$$\sigma(v) = \begin{cases} 0, & \text{if } v < v_0 \\ \sigma_0(v) \left[1 - \left(\frac{v_0}{v}\right)^2\right], & \text{if } v > v_0 \end{cases} \quad (8)$$

with

$$v_0 = \frac{u_{rms}}{2}, \quad (9)$$

$$\sigma_0(v) = \pi a_B^2 Z_{ef}^2(v) \left(\frac{1}{vv_0}\right)^2, \quad (10)$$

and

$$Z_{ef}(v) = Z_T \left[1 - 1.08 \exp(-80.1 Z_T^{-0.506} (v/c)^{0.996})\right], \quad (11)$$

where  $a_B$  is the Bohr radius,  $c$  is the velocity of light, and  $Z_T$  is the target atomic number. For anions, the Bohr-Lindhard's threshold velocity is parameterized in terms of the Electron Affinity (EA) [40, 41] as

$$v_0 = \frac{1}{2} \sqrt{\frac{EA(eV)}{13.6}}. \quad (12)$$

In Fig. 4 we also show the results from Eq. (8) for  $O^- + N_2$ . The agreement with experimental data is poor, for two reasons: (i) The modeling of the target as a dressed charged particle is a naive approximation to a much more complex problem [42], and is especially inadequate for collision between an electron and the  $N_2$  target [17]. (ii) The value for the free-collision threshold is overestimated due to neglecting the velocity of the ionized electron within the projectile frame of reference. Variations of the FCM deal with these limitations by including a combination of previously known cross sections for electron-impact elastic scattering by the target and the projectile electronic-velocity distribution (e.g. [43–46]).

This more general FCM approach includes a velocity threshold for the electron detachment, since there is still a maximum momentum that the massive target can transfer to the projectile's electron. This limit is now affected by the angular dependence of elastic scattering of a free electron by the target and by the electronic distribution of the anionic projectile [46–48]. An onset for detachment cross sections is expected as the projectile velocity increases, although a velocity threshold convoluted with the projectile internal velocity distribution.

However, quadruple integrals involved if this approach are a limitation to FCM calculations of cross sections involving anionic projectiles and molecular targets, often restricted to the intermediate-to-high velocity regime

(*e.g.* [24, 25, 46–51]). In the present work, we combine the Bohr-Lindhard's approach with a threshold analysis of the general Risselman's approach in order to obtain a simple analytical expression of the FCM threshold behavior that takes into account the electronic velocity distribution within the projectile.

In Risselmann's formulation of the FCM [46], the total-electron-loss cross section  $Q(v_N)$  for a one-electron projectile for which the nucleus has a velocity  $\mathbf{v}_N = v_N \hat{z}$  is given by

$$\int_0^\infty f(u) du \int_0^\pi \frac{1}{2} \sin(\beta) d\beta \int_0^{2\pi} d\phi \int \sigma(v, \theta) \sin(\theta) d\theta, \quad (13)$$

where  $u$  and  $\beta$  are, respectively, the modulus and the angle with  $z$  axis of the projectile electron in the projectile frame of reference, and  $v$  is the velocity of the same electron, but in the laboratory frame of reference.  $f(u)$  is the distribution of absolute values of the velocity of the projectile's electron.  $\sigma(v, \theta)$  is the differential electron-scattering cross section at an angle  $\theta$  for a free electron impinging on the target. For elastic collisions,  $\Delta E = 0$ , Risselmann's expression of the inequality regarding energy and momentum conservation reduces to

$$(v_N + u \cos(\beta))(1 - \cos(\theta)) + u \sin(\beta) \cos(\phi) \sin(\theta) \geq u_{rms}^2 / (2v_N), \quad (14)$$

where the characteristic anion velocity  $u_{rms}$  is obtained from  $EA = mu_{rms}^2/2$ . While  $u_{rms}$  is often interpreted as a root mean squared value, it is normally obtained from experimental EA values [46–48]. Near threshold, close collisions are most relevant to higher momentum transfer. Thus, we approximate  $\theta \approx \pi$  and, using  $v_0 = u_{rms}/2$ , obtain from Eq. (14)

$$\frac{v_N}{v_0} \left( \frac{v_N}{v_0} + \frac{u}{v_0} \cos(\beta) \right) \geq 1. \quad (15)$$

If the electron velocity in the projectile frame of reference ( $u$ ) is negligible compared to the anion nucleus velocity, then  $v_N \geq v_0$  and  $v_0$  is the threshold velocity (as in the Bohr-Lindhard's approach). Otherwise, Eq. (15) results in a threshold velocity that is a function of the product  $u \cos(\beta)$ , which is the  $z$  component of the electron velocity within the anion,  $u_z$ . Defining  $s = v_N/v_0$  and  $t = u/v_0$  We can write

$$t \cos(\beta) \geq \left( \frac{1}{s} - s \right) \quad (16)$$

The particular case  $\cos(\beta) = \pm 1$  gives electron momentum parallel or anti-parallel to the anion's nucleus

velocity, resulting in the  $s$  positive limit solutions

$$s_{<} = \sqrt{1 + \left(\frac{t}{2}\right)^2} - \frac{t}{2}, \quad (17)$$

$$s_{>} = \sqrt{1 + \left(\frac{t}{2}\right)^2} + \frac{t}{2}. \quad (18)$$

If the distribution  $f(u) = \delta(u - u_{rms})$  then  $t = 2$ , and therefore  $s_{<} = \sqrt{2} - 1$  and  $s_{>} = \sqrt{2} + 1$ . Thus, within the  $\delta$  approximation for  $f(u)$ ,

$$v_{<} = (\sqrt{2} - 1) v_0 \approx 0.414 \frac{1}{2} \sqrt{\frac{EA(eV)}{13.6}}. \quad (19)$$

The ratio  $R$  between cross section for projectile electron loss  $\sigma_{O^-}$  and total electron elastic cross sections  $\sigma_e$  can be used to compare experimental data to the FCM results. Within the Bohr-Lindhard's approach, assuming  $\sigma_0 = \sigma_e$ , this leads to an expression unaffected by the dressed-charge approximation to the target:

$$R_{B-L} = 1 - \left(\frac{v_0}{v}\right)^2. \quad (20)$$

We substitute the Bohr-Lindhard's threshold velocity by  $v_{<}$  (Eq. 19) and obtain

$$R = 1 - \left(\frac{(\sqrt{2} - 1) v_0}{v}\right)^2. \quad (21)$$

Figure 5 shows ratios of  $O^- + N_2$  projectile electron loss to the  $e^- + N_2$  total electron elastic cross sections of Kitajima *et al.* [33]. For sufficiently high velocities, the FCM predicts a ratio of 1. The ratios for the higher-energy data of Matic [26], with velocities in the range between  $v_0$  and  $u_{rms}$ , are close to one.

We show in Fig. 5 the FCM results obtained from the B-L approach (Eq. 20) and and the B-L result with threshold velocity  $v_0$  replaced by the  $v_{<}$  expression obtained in the present work (Eq. 21). We represent the range of velocities with  $\beta$  integration restrictions (Eq. 16) by the grey shaded area. The comparison between the two FCM results and the experimental data, both from this work and from Matic and Cobic [26], shows that the substitution of the threshold velocity  $v_0$  by  $v_{<}$  results in good FCM description of the anionic-projectile collision system studied in the present work. It also suggests that for anionic projectiles (for which the EA values are at most of a few eV), even close to the FCM threshold, the  $\beta$  distribution are more relevant to cross-section convolution that the distribution of absolute values  $u$  (see Eq. 13). The parametrization of  $R$  only on EA, via  $v_{<}$ , provides a contribution in the pursue of scaling laws common to few-keV projectile-electron-loss cross sections for anionic projectiles (*e.g.* [11, 13–16]).

It is important to note that the existence of the threshold for quasi-free electron detachment doesn't imply that

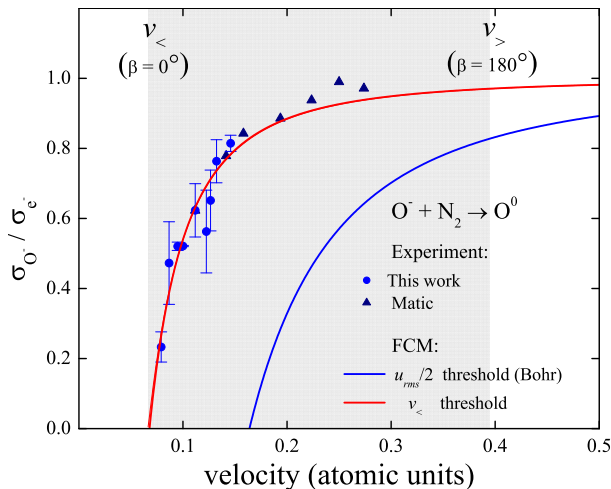


FIG. 5. Ratio of cross sections for  $O^- + N_2$  projectile electron loss and total electron scattering by  $N_2$  (using  $e^- + N_2$  of Kitajima [33]). Closed circles, present SGR data; closed up triangles, Matic and Cobic [26]; Blue line, Bohr-Lindhard FCM; Red line, modification of Bohr-Lindhard FCM with the  $v_<$  velocity threshold; The grey shaded area highlights the velocity range with threshold affected (within the FCM) by the angle  $\beta$  between the incidence direction and projectile electron direction. The region is delimited by  $v_<$  ( $\beta = 0$ ) and  $v_>$  ( $\beta = 180$  deg).

the projectile-electron-detachment cross section is expected to be zero below threshold. At very low velocities, molecular states formed by projectile and target can result in large cross sections [52]. In the case of  $O^- + N_2$  those states are related to the temporary formation of a  $N_2O^-$  complex [53]. The velocity dependence of projectile-electron-detachment cross sections with a peak before threshold was observed, for example, in  $O_2^- + N_2$  collisions [54].

#### IV. CONCLUSIONS

The total projectile-electron-loss cross sections for  $O^- + N_2$  in the energy range from 2.5 to 8.5 keV have been measured with two methods: the beam attenuation ( ${}^b\sigma_{-10}$ ) and the signal growth rate techniques

( ${}^s\sigma_{-10}$ ). Close to this energy range, previously published cross sections show a long-standing considerable disagreement, depending on the measurement method used. The present data have also shown this discrepancy between results originated in different methods. At the same time, for each method, the present results are consistent with the cross sections measured with corresponding techniques. We propose that this discrepancy can be explained by the presence of auto-detaching metastable states that cause  ${}^b\sigma_{-10}$  to be larger. This hypothesis may solve the aforementioned disagreement.

From a fundamental point of view, a negative ion can be considered a simple carrier to a free electron under certain circumstances. The free collision model (FCM) is based on this assumption. However, the validity of this model close to the velocity threshold has been rarely assessed. In this study, we present a general, simple, and analytical expression for the velocity threshold within the FCM, easily applied for anionic projectiles. When applied to the  $O^- + N_2$  collision system, the expression shows consistency with the experimental threshold value obtained from the velocity dependence of our data.

In addition to its fundamental interest, in plasma modeling, electron scattering is a very important process given the abundance of electrons and the impact of this process on the plasma electron density function. In this work, we demonstrate that the process of electron loss from  $O^-$  at a speed  $v$  above  $\sim 0.25$  a.u. the cross section for electron detachment is as relevant as electron scattering and in a given plasma environment with a high density of negative ions, such as carbohydrate plasma, electron detachment could be even more relevant than electron scattering.

#### ACKNOWLEDGEMENTS

G. H. acknowledges the National Autonomous University of Mexico (UNAM) through the Support Program for the Improvement of the Academic Staff of UNAM (PASPA). Technical support from Guillermo Bustos, Héctor H. Hinojosa, Reyes García, Armando Bustos, Juana A. Romero and Arturo Quintero is acknowledged. This study was supported in part by the Brazilian agency Fundação de Amparo à Pesquisa do Estado do Rio de Janeiro (FAPERJ), code E-262109342019 and in part by CONAHCYT CF-2023-I-918.

- 
- [1] A. Ramírez-Solís, J. Vigué, G. Hinojosa, and H. Saint-Martin, Solving the  $CH_4^-$  riddle: The fundamental role of spin to explain metastable anionic methane, *Phys. Rev. Lett.* **124**, 056001 (2020).  
 [2] M. J. Jensen, U. V. Pedersen, and L. H. Andersen, Stability of the ground state vinylidene anion  $H_2CC^-$ ,

- Phys. Rev. Lett.* **84**, 1128 (2000).  
 [3] Y. V. Medvedev, Acceleration and trapping of ions upon collision of ion-acoustic solitary waves in plasma with negative ions, *Plasma Phys. Rep.* **45**, 230 (2019).  
 [4] A. Mondal, S. V. Rahul, R. Gopal, D. Rajak, M. Anand, J. Jha, S. Tata, A. K. Dharmadhikari,

- A. K. Gupta, and M. Krishnamurthy, Misjudging negative ions for electrons in intense laser plasma diagnostics, *AIP Advances* **9**, 025115 (2019).
- [5] A. J. Coates, F. J. Crary, G. R. Lewis, D. T. Young, J. H. W. Jr., and E. C. S. Jr., Discovery of heavy negative ions in titan's ionosphere, *Geophys. Res. Lett.* **34**, L22103 (2007).
- [6] M. A. Cordiner and S. B. Charnley, Negative ion chemistry in the coma of comet 1p/halley, *Meteoritics & Planetary Science* **7**, 1 (2013).
- [7] L. B. Strogonova, A. E. Sorokin, Y. A. Vasin, and A. E. Belyavskii, Creating an atmosphere within spacecraft, *Russ. Engin. Res.* **39**, 813 (2019).
- [8] R. C. Fortenberry, Interstellar anions: The role of quantum chemistry, *J. Phys. Chem. A* **119**, 9941 (2015).
- [9] M. Khamesian, N. Douguet, S. F. dos Santos, O. Dulieu, M. Raoult, W. J. Brigg, and V. Kokoouline, Formation of  $CN^-$ ,  $C_3N^-$ , and  $C_5N^-$  molecules by radiative electron attachment and their destruction by photodetachment, *Phys. Rev. Lett.* **117**, 123001 (2016).
- [10] E. M. Hernández, L. Hernández, C. Martínez-Flores, N. Trujillo, M. Salazar, A. Chavez, and G. Hinojosa, Electron detachment cross sections of  $CH_4^-$  colliding with  $O_2$  and  $N_2$  below 10keV energies, *Plasma Sources Sci. T.* **23**, 015018 (2014).
- [11] F. Zappa, G. Jalbert, L. F. S. Coelho, A. B. Rocha, S. D. Magalhães, and N. V. d. Castro Faria, Absolute electron detachment cross sections of atomic anions of the second and third periods incident on noble gases, *Phys. Rev. A* **69**, 012703 (2004).
- [12] A. C. F. Santos and R. D. DuBois, Scaling laws for single and multiple electron loss from projectiles in collisions with a many-electron target, *Phys. Rev. A* **69**, 042709 (2004).
- [13] S. Wu, X. Zhanga, and G. Li, Single-electron detachment cross sections for negative ions of transition elements colliding with gases, *At. Data and Nucl. Data Tables* **93**, 575 (2007).
- [14] Z. Geng, X. Bai, B. Wei, and X. Zhang, Single-electron detachment cross sections of co- and ir- in collision with ar and an empirical formula for single-electron detachment cross sections of negative ions in collision with ar, *Can. J. Phys.* **91**, 175 (2013), <https://doi.org/10.1139/cjp-2012-0278>.
- [15] G. Min, G. Guo, D. Wang, and X. Zhang, Single-electron-detachment cross sections of  $Fe^-$ ,  $Ru^-$ ,  $Ni^-$ ,  $Pd^-$ , and  $Pt^-$  in collisions with inert-gas atoms, *Phys. Rev. A* **95**, 062706 (2017).
- [16] Y. Yang, J. Wang, Y. Tian, and X. Zhang, Single and double electron detachment absolute cross sections of  $h^-$  and  $d^-$  in collisions with  $SF_6$  and  $CF_4$ , *Can. J. Phys.* **100**, 272 (2022), <https://doi.org/10.1139/cjp-2022-0017>.
- [17] M.-Y. Song, H. Cho, G. P. Karwasz, V. Kokoouline, and J. Tennyson, Electron scattering on molecular nitrogen: common gas, uncommon cross sections, *Eur. Phys. J. D* **77**, 105 (2023).
- [18] E. Hernández and G. Hinojosa, Collision induced electron detachment cross sections of the  $H_2CC^-$  anion below 10 keV on  $O_2$  and  $N_2$ , *Int. J. Mass Spectrom.* **424**, 35 (2018).
- [19] A. Lira, A. Martínez, A. Escalante, S. Vergara, and G. Hinojosa, Electron loss of  $CH^-$  and  $CH_2^-$  induced by interactions with  $N_2$  and  $O_2$  at keV energies, *Int. J. Mass Spectrom.* **469**, 116681 (2021).
- [20] A. A. M. S Vergara, F. R. P. nalver, and G. Hinojosa, Electron detachment cross section of  $H^-$  induced by collisions with  $O_2$ , *J. Phys. B: Atom. Molec. Phys.* **54**, 10.1088/1361-6455/ac1646 (2021).
- [21] M. Salazar-Zepeda, C. Gleason, E. González, O. G.-M. na, and G. Hinojosa, Double electron capture by protons in collisions with  $H_2$ , *Nucl. Instrum. Meth. B* **268**, 1558 (2010).
- [22] J. S. Allen, X. D. Fang, A. Sen, R. Matulioniene, and T. J. Kvale, Double-electron detachment cross sections in intermediate-energy  $H^-$  plus noble-gas collisions, *Phys. Rev. A* **52**, 357 (1995).
- [23] M. E. W, M. J. B. A, and R. M. E, *Atomic Collisions, Heavy Particle Projectiles* (John Wiley & Sons, Inc., New York, NY (United States), 605 Third Avenue, New York, NY, 1993).
- [24] R. F. Nascimento, S. L. A. Mello, B. F. Magnani, M. M. Sant'Anna, G. Jalbert, and N. V. de Castro Faria, Total detachment cross sections of  $C^-$ ,  $CH^-$ ,  $C_2^-$ , and  $C_2H^-$  incident on  $N_2$  at keV energies., *Phys. Rev. A* **87**, 062704 (2013).
- [25] G. Jalbert, R. F. Nascimento, C. R. de Carvalho, C. R. Carvalho, B. F. Magnani, A. C. F. Santos, A. B. Rocha, M. M. Sant'Anna, and N. V. de Castro Faria, Electron-detachment cross section for  $CN^-$  and  $O_2^-$  incident on  $N_2$  at intermediate velocities, *Phys. Rev. A* **89**, 012712 (2014).
- [26] M. Matic and B. Cobic, Electron loss by  $C^-$  and  $O^-$  ions in gaseous targets, *J. Phys. B: Atom. Molec. Phys.* **4**, 111 (1971).
- [27] R. A. Bennett, J. T. Moseley, and J. R. Peterson, Electron loss cross sections for  $O^-$ ,  $O_2^-$ ,  $NO_2^-$ , and  $NO_3^-$  in several gases, *J. Chem. Phys.* **62**, 2223 (1975).
- [28] F. Rahman and B. Hird, Electron detachment atomic cross sections from negative ions, *At. Data and Nucl. Data Tables* **35**, 123 (1986).
- [29] E. Hernández, L. Hernández, L. Serkovic-Loli, and G. Hinojosa, Collisional induced double electron loss of  $NO^-$  and  $CH_4^-$  anions below 10 keV energies, *Int. J. Mass Spectrom.* **403**, 39 (2016).
- [30] J. Ishikawa, H. Tsuji, and T. Maekawa, Electron detachment cross-sections in low energy heavy negative ion beam apparatus, *Vacuum* **39**, 1127 (1989).
- [31] M. Halka, P. G. Harris, A. H. Mohagheghi, R. A. Reeder, C. Y. Tang, H. C. Bryant, J. B. Donahue, and C. R. Quick, Electric-field effects on  $H^-$  photodetachment partial cross sections above 13.4 eV, *Phys. Rev. A* **48**, 419 (1993).
- [32] H. Tsuji, J. Ishikawa, T. Maekawa, and T. Takagi, Electron detachment cross-sections for heavy negative-ion beam, *Nucl. Instrum. Meth. B* **37-38**, 231 (1989).
- [33] M. K. et al., Low-energy and very-low energy total cross sections for electron collisions with  $n_2$ , *Eur. Phys. J. D* **71**, 139 (2017).
- [34] B. G. Lindsay, W. S. Yu, K. F. McDonald, and R. F. Stebbings, Electron capture and loss by kilo-electron-volt oxygen atoms in collisions with he,  $H_2$ ,  $N_2$ , and  $O_2$ , *Phys. Rev. A* **70**, 042701 (2004).
- [35] I. M. Fogel, V. Ankudinov, and D. Pilipenko, Electron capture and loss in collisions of fast carbon and oxygen atoms with gas molecules, *Sov. Phys. JETP* **8**, 601 (1959).



- [36] N. Bohr, The penetration of atomic particles through matter, *Dan. Vidensk. Selsk. Mat.-Fys. Medd.* **18**, 1 (1948).
- [37] N. Bohr and K. Lindhard, Electron capture and loss by heavy ions penetrating through matter, *Dan. Vidensk. Selsk. Mat.-Fys. Medd.* **28**, 1 (1954).
- [38] T. Niklaus, G. Bonani, Z. Guo, M. Suter, and H.-A. Synal, Optimising tandem accelerator stripping efficiency by simulation of charge changing processes, *Nucl. Instrum. Meth. B* **92**, 115 (1994).
- [39] R. O. Sayer, Semi-empirical formulas for heavy-ion stripping data, *Rev. Phys. Appl. (Paris)* **12**, 1543 (1977).
- [40] M. K. K. et al., High-precision electron affinity of oxygen, *Nat Commun* **13**, 5906 (2022).
- [41] C. Ning and Y. Lu, Electron Affinities of Atoms and Structures of Atomic Negative Ions, *J. Phys. Chem. Ref. Data* **51**, 021502 (2022), <https://pubs.aip.org/aip/jpr/article-pdf/doi/10.1063/5.0080243/13529567/02150215021502.pdf>.
- [42] E. Montenegro, W. Meyerhof, and J. McGuire, Role of two-center electron-electron interaction in projectile electron excitation and loss (Academic Press, 1994) pp. 249–300.
- [43] D. Bates and J. Walker, Quenching of auroral hydrogen line emission by collisional ionization, *Planetary and Space Science* **14**, 1367 (1966).
- [44] D. Bates and J. Walker, A classical impulse approximation treatment of collisional detachment from h-ions, *Proceedings of the Physical Society* **90**, 333 (1967).
- [45] D. Bates, V. Dose, and N. Young, Classical treatment of electron loss, *Journal of Physics B: Atomic and Molecular Physics* **2**, 930 (1969).
- [46] K. Riesselmann, L. W. Anderson, L. Durand, and C. J. Anderson, Classical impulse approximation for the electron loss from H(1s) or H<sup>−</sup> projectiles passing through various gas targets, *Phys. Rev. A* **43**, 5934 (1991).
- [47] G. M. Sigaud, Free-collision model calculations for the electron detachment of anions by noble gases, *J. Phys. B: Atom. Mol. Phys.* **41**, 015205 (2008).
- [48] G. M. Sigaud, Free-collision model calculations for projectile electron loss by the H<sub>2</sub> molecule, *J. Phys. B: Atom. Mol. Phys.* **44**, 225201 (2011).
- [49] P. H. J. Heinemeier and F. R. Simpson, Collisional detachment cross sections for H<sup>−</sup> and He<sup>−</sup> at high energies, *J. Phys. B: Atom. Mol. Phys.* **9**, 2669 (1976).
- [50] M. M. Sant'Anna, F. Zappa, A. C. F. Santos, A. L. F. de Barros, W. Wolff, L. F. S. Coelho, and N. V. de Castro Faria, Electron-detachment cross sections of halogen negative-ion projectiles for inertial confinement fusion, *Plasma Phys. Contr. Fusion* **46**, 1009 (2004).
- [51] M. M. Sant'Anna, F. Zappa, G. Jalbert, A. C. F. Santos, B. F. Magnani, L. F. S. Coelho, , and N. V. de Castro Faria, Electron-loss cross sections for heavy-ion beam probe using gold beams: experiment and theory, *Plasma Phys. Contr. Fusion* **51**, 045007 (2009).
- [52] V. A. Esaulov, Electron detachment from atomic negative ions, *Ann. Phys. Fr.* **11**, 493 (1986).
- [53] J. Comer and G. J. Schulz, Measurements of electron-detachment cross sections from O<sup>−</sup> and S<sup>−</sup>, *Phys. Rev. A* **10**, 2100 (1974).
- [54] M. Mendes, C. Guerra, A. I. Lozano, D. Rojo, J. C. Oller, P. Limão-Vieira, and G. García, Experimental electron-detachment cross sections for collisions of O<sub>2</sub><sup>−</sup> with N<sub>2</sub> molecules in the energy range 50-7000 eV, *Phys. Rev. A.* **99**, 062709 (2019).